Latitude-Longitude Grid Suitable for Numerical Time Integration of a Global Atmospheric Model

J. LEITH HOLLOWAY, JR., MICHAEL J. SPELMAN, and SYUKURO MANABE

Geophysical Fluid Dynamics Laboratory,[1] *NOAA, Princeton, N.J.*

ABSTRACT—A simple, free-surface, barotropic model and a nine-level, baroclinic model are numerically time integrated on both latitude-longitude grids and on Kurihara-type grids to compare the results obtained from the two grid systems. The prognostic variables are Fourier space-filtered in the longitudinal direction on the latitude-longitude grids to permit the use of the same time-step length on both grids.

With respect to geopotential height and zonal wind distributions and to the phase speed of wave propagation, the results from the barotropic model, time-integrated on a sector latitude-longitude grid, agree better with a high-resolution control run than those computed on a modified Kurihara grid, particularly at high latitudes.

The barotropic model is also time-integrated on a hemispheric, latitude-longitude grid, and the results compare well with a high-resolution control. The latter comparison is performed on initial data having strong cross-polar flow.

The mean sea-level pressure distribution obtained from a 64-day time integration of the baroclinic model on a global, latitude-longitude grid is better than that derived from a similar model using a Kurihara grid of comparable resolution. For example, the tendency for the Kurihara grid model to predict excessive pressures in the north polar region is for the most part corrected by use of the latitude-longitude grid.

1. INTRODUCTION

Time integrations of the equations for atmospheric motion over the whole globe encounter special problems because no projection scheme is available for representing the entire surface of a sphere on a single plane without prohibitive distortion in some areas. Kurihara and Holloway (1967) integrated a nine-level, primitive-equations model on a global grid system proposed by Kurihara (1965). Holloway and Manabe (1971) have pointed out problems that arise when the Kurihara grid is used for a long-period time integration of a global general circulation model. For example, excessive high pressure develops in polar regions and low- and high-pressure belts systematically shifted toward the Equator.

We think that these deficiencies arise primarily because there are not enough gridpoints to resolve the curvature of the coordinate system in latitude circles near the poles. These difficulties may also be partly a consequence of the staggered positioning of grid boxes in the Kurihara grid.

An obvious solution to these problems is to use a grid defined as the intersections of latitude circles with meridians where the increments of latitude and longitude are nearly identical. However, a very short time step is required to insure computational stability on this grid because the east–west separation of grid points is very small near the poles. A time step short enough for stability in polar regions is wastefully short in low latitudes, and time integrations on this grid would, therefore, be exceedingly expensive unless this shortcoming can be overcome.

Grimmer and Shaw (1967) tested this latitude-longitude grid by using a time step that is a function of latitude. They interpolated the predicted variables in time to link the different time levels that resulted from the variable time steps.

A more practical approach to this problem has been to filter out the short waves that cause the computational instability near the poles so that a uniform time step of practical length can be used throughout the grid. Mintz and Arakawa (Gates et al. 1971) filtered the zonal mass-flux variables and the zonal pressure gradient terms in the model equations. This filtering is accomplished by weighted averaging of these terms along latitude circles. The filter is designed in such a way that the degree of smoothing increases towards the poles.

Umscheid and Sankar-Rao (1971) used Fourier filtering for damping high wave-number components in the zonal fluxes and pressure gradient terms in their model computed on a modified Kurihara grid with considerably higher east–west resolution near the poles. This filtering permits the use of the same time-step length over the entire globe, despite the decreasing east–west grid spacing along latitude circles as the poles are approached. It is not possible, however, to determine the overall scale of the truncation when filtering is not applied uniformly to all terms in the tendency equations.

On the other hand, Vanderman (1970) used running means to filter high wave-number components from total tendencies computed by his barotropic model integrated on a global, latitude-longitude grid. As explained in the next section, this filtering method can cause computational instability under some circumstances.

The purpose of our work is to test the accuracy and

---

[1] At Forrestal Campus of Princeton University

stability of solutions of hydrodynamical equations solved on latitude-longitude grids with Fourier filtering of the basic prognostic variables. For ease in interpreting the results, we ruled out the practice of filtering only selected terms in the model equations. These experiments are carried out on both a barotropic and a baroclinic model.

2. FOURIER FILTERING

To prevent linear instability from occurring in the time integration on the latitude-longitude grid, we applied space filtering to all time-integrated variables at each time step. Otherwise, a progressively shorter time-step length would have to be used as the time integration advances towards the poles, where the east–west gridpoint spacing becomes smaller (Grimmer and Shaw 1967). The filtering methods adopted in this study limit the east–west wavelength of the shortest wave at any latitude to approximately two grid distances at the Equator. The fact that this permits stable time integrations is proved in appendix 1. The minimum wavelength, L_{min} is specified as

$$L_{min} = 4\pi a N^{-1} \qquad (1)$$

where a is the radius of the earth and N is the number of gridpoints in a latitude circle. This minimum wavelength is guaranteed by limiting the maximum wave number in the data at any latitude, θ, to

$$k_{max} = 2\pi a L_{min}^{-1} \cos \theta = \frac{1}{2} N \cos \theta. \qquad (2)$$

In practice, k_{max} must, of course, be rounded to the nearest integer; and L_{min} is thereby slightly altered.

This space filtering is accomplished by analyzing the data along each latitude circle into their Fourier components and resynthesizing the data with only the desired waves present. Effectively, no filtering is done at the Equator. It can be shown that this filtering scheme has no significant effect on the quadratic conserving properties of finite-difference equations because the truncated components are orthogonal to the retained ones.

According to our tests, the Fourier filtering method is better than the running-mean method proposed by Vanderman (1970) in one important respect. As pointed out by Holloway (1958), a running-mean filter can reverse the polarities of some short waves in addition to reducing their amplitudes. This can cause computational instability at the wavelength of the negative response in a time integration of a model with frictional damping. Once a wave of this length is introduced into the flow, it cannot be removed because the running mean would reverse any tendency to suppress it; and, therefore, this wave would grow without bound. On the other hand, Fourier filtering removes all short wavelengths completely without any positive or negative residuals. Whereas it may be possible to time integrate a simple barotropic model on a latitude-longitude grid with running-mean filters (as Vanderman did), the negative response characteristics of equally weighted running averages would prohibit the stable time integration of a model with frictional damping.

The magnitude of the negative response discussed here can be minimized by using a numerical filter that has unequal weights proportional to the ordinates of a normal curve. However, the results of a test with a barotropic model show that this filter tends to suppress the development of cutoff Lows, as discussed in section 4.[2]

In the case of vector variables, we consider it desirable to transform the components to a polar stereographic projection before the Fourier filtering is performed. Without this transformation, a Fourier analysis of vector components around an entire latitude circle may introduce errors in cases where there is significant flow across the poles. As first pointed out by Shuman (1970), the process of averaging two vector components in spherical coordinates at two widely separated longitudes can produce serious error near the poles because of the large difference in the directions of the unit vectors. Therefore, before the Fourier filtering is done on vector components, they are transformed into components in the directions of a set of two orthogonal unit vectors on a polar stereographic projection plane.

The stereographic components, U_s and V_s, are computed as follows:

$$U_s = -u \sin \lambda - v \cos \lambda \qquad (3)$$

and

$$V_s = u \cos \lambda - v \sin \lambda \qquad (4)$$

where u and v are the zonal and meridional components of the vectors, respectively, and λ is the longitude. The final vector components for use by the model are derived by transforming the filtered stereographic components, $\overline{U}_s$ and $\overline{V}_s$, back to spherical coordinates as follows:

$$\overline{u} = -\overline{U}_s \sin \lambda + \overline{V}_s \cos \lambda \qquad (5)$$

and

$$\overline{v} = -\overline{U}_s \cos \lambda - \overline{V}_s \sin \lambda \qquad (6)$$

where the overbar signifies Fourier-filtered variables. The above formulas apply only to a northern hemispheric projection. They can be altered for the Southern Hemisphere by changing the sign of u and $\overline{u}$ everywhere.

3. DESCRIPTION OF THE BAROTROPIC MODEL

The primitive equations of motion for divergent barotropic flow in an inviscid, incompressible fluid are solved by finite-difference methods. The equations in flux form and in spherical coordinates are as follows:

$$\frac{\partial hu}{\partial t} = -\frac{\partial hu^2}{a \cos \theta \partial \lambda} - \frac{\partial huv \cos \theta}{a \cos \theta \partial \theta}$$
$$+ (f + a^{-1}u \tan \theta)hv - gh\frac{\partial h}{a \cos \theta \partial \lambda}, \qquad (7)$$

---

[2] Vanderman (1972) has recently experimented with unequally weighted filters in which the weights decrease linearly from a central maximum value.
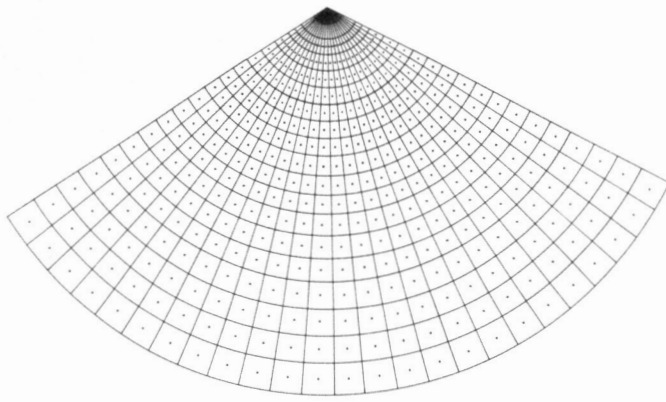
FIGURE 1.—Low-resolution sector latitude-longitude grid projected on a polar stereographic plane.

FIGURE 2.—Polar stereographic projection of the modified Kurihara grid.

$$\frac{\partial hv}{\partial t} = -\frac{\partial huv}{a\cos\theta\partial\lambda} - \frac{\partial hv^2\cos\theta}{a\cos\theta\partial\theta}$$
$$-(f+a^{-1}u\tan\theta)hu - gh\frac{\partial h}{a\partial\theta}, \qquad (8)$$

and

$$\frac{\partial h}{\partial t} = -\frac{\partial hu}{a\cos\theta\partial\lambda} - \frac{\partial hv\cos\theta}{a\cos\theta\partial\theta} \qquad (9)$$

where h is the height of the free surface in geopotential units, f is twice the vertical component of the earth's rotation, t is time, g is the acceleration of gravity, and the other variables are as previously defined. See appendix 2 for the finite-difference versions of these equations.

These equations are first solved in a domain that covers a third of a hemisphere (120° in longitude). There is cyclic continuity at the eastern and western boundaries and a free-slip condition at the Equator (southern boundary).

The barotropic model is time integrated by the leap-frog method with a time step of 10 min except for the high-resolution control experiments to be described later. As insurance against the development of excessive gravity waves in the time integrations of this model, however, the so-called Euler-backward time differencing scheme (Matsuno 1966, Manabe et al. 1970) is used periodically for eight consecutive time steps. This scheme is applied once approximately every day in the low-resolution time integrations and once every 1/4 day at high resolution. For further discussion on the computational aspects of this work, see appendix 3.

4. COMPARISON OF BAROTROPIC MODEL RESULTS WITH DIFFERENT GRIDS

To test the performance of the proposed new grid system, we integrated the barotropic model with respect to time on three grid systems: a latitude-longitude grid, a modified Kurihara grid, and a high-resolution, latitude-longitude or control grid. The low-resolution, latitude-longitude grid is shown in figure 1. The grid points are represented as dots at the centers of the trapezoid-shaped boxes. The dots are omitted from the northernmost two rows of boxes because of lack of space. There are 25 gridpoints in each latitude-circle segment, which spans 120° of
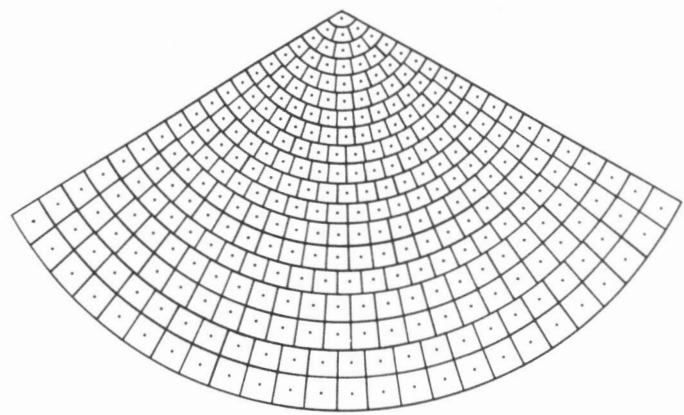
TABLE 1.—*Maximum wave number per sector* ($k_{max}/3$) *versus latitude and the corresponding effective east-west grid spacing* ($L_{min}/2$) *for the barotropic model using the sector latitude-longitude grid*

Latitude	$k_{max}/3$	$L_{min}/2$
(deg.)		(km)
2.4	12	556
7.1	12	552
11.8	12	544
16.6	12	533
21.3	11	565
26.1	11	545
30.8	10	573
35.5	10	543
40.3	9	566
45.0	9	524
49.7	8	539
54.5	7	554
59.2	6	569
63.9	5	586
68.7	4	606
73.4	3	635
78.2	2	685
82.9	1	825
87.6	0	∞

longitude, in the domain of this model integration. There are 19 latitude circles, and the southern boundary of the outer row of boxes is the Equator. Therefore, there are 475 gridpoints in the field.

The maximum wave number per sector permitted by the filtering procedure at each latitude of the latitude-longitude grid is given in table 1. For each wave number listed in this table, there is a corresponding minimum wavelength, L_{min}. Half of this wavelength, which can be regarded as an effective east-west grid distance, is also listed in table 1. The north-south grid spacing is 527 km everywhere in this grid.

As a comparison with the results obtained from the above grid, the barotropic model equations were also integrated on the modified Kurihara grid shown in figure 2. On the original global Kurihara grid, the number of points on any given latitude circle is four greater than on the adjacent latitude circle toward the pole. The boxes are

almost square near the Equator, but they become elongated in the east–west direction near the poles. On the modified Kurihara grid, the number of gridpoints in each latitude circle is adjusted so that the boxes are nearly square everywhere, and the east–west resolution closely matches the north–south spacing at all locations in the grid. The nearly constant grid distance averages about 530 km. There are 302 gridpoints in a 120° sector of this modified Kurihara grid.

To obtain a better estimate of the true solution to the time integration of the model, we integrated the model equations on a sector latitude-longitude grid with double the resolution of the latitude-longitude grid mentioned previously. This high-resolution grid has 38 rows and 1,900 points. The double-resolution, latitude-longitude grid should give a solution close enough to the actual to serve as an adequate standard for gaging the accuracy of the low-resolution runs. To avoid complicating the analysis, we performed the high-resolution control integration without space filtering so that a very short time step (12 s) was required to insure stability.

The initial conditions for these experiments are those used by Phillips (1959), except that the wave number specified is 6 instead of 4. The initial geopotential height is given as a function of θ and λ and is shown in figure 3. The velocity components are computed from a stream function that is consistent with the heights in the continuum. However, since the initial u and v components are computed from the analytic stream function by the same finite-difference operators as used in the time integration of the model, they are slightly out of balance with the analytically derived height field because of truncation error. Undoubtedly, this contributed to the generation of gravity waves in the subsequent time integration.

According to the analytic solution to these initial conditions, the waves should propagate eastward at a rate of 24.6°/day without change in shape. The analytic solution applies, however, to the case of nondivergent flow. Therefore, the phase speed of waves in the free-surface barotropic model integrated here will be only approximately this value.

The geopotential height fields at 3 and 6 days for the time integrations on the three grid systems are compared in figure 4. If we assume that the high-resolution experiment (figs. 4A, 4D) is the most accurate time integration, the true divergent model solution has cutoff Low centers developing, rather than troughs merely moving without change in shape as the theory for nondivergent flow predicts. The low-resolution, latitude-longitude grid integration (figs. 4B, 4E) develops in close agreement with the control run except that there is significant retardation in trough location by the 6th day. On the other hand, the systems show considerable slowing in the modified Kurihara-grid integration (figs. 4C, 4F), and the flow pattern becomes irregular by the 6th day. Furthermore, the flow in the modified Kurihara-grid run tends to become more zonal than the integrations on the latitude-longitude grids. Some irregularities occur in the latitude-longitude
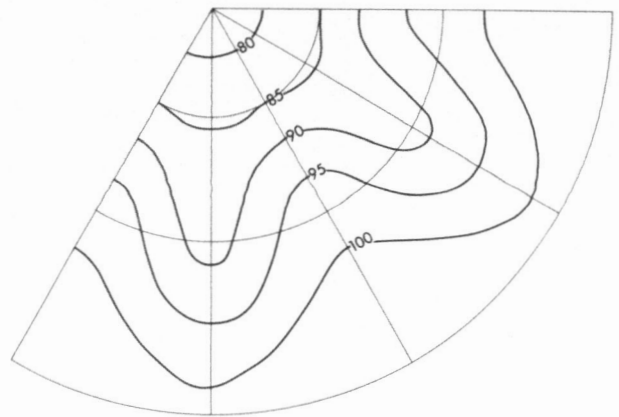
FIGURE 3.—Initial distribution of free-surface geopotential height in units of 102.04 gpm (100 dynamic m).

grid results near the Equator (fig. 4E). The reason for these irregularites is yet to be identified.

Earlier experiments using filters with normal curve weighting suffered from retarded and suppressed development of cutoff Low centers. The Fourier filtering permits a more realistic development of the flow as indicated by the favorable comparison of the latitude-longitude grid run shown in figures 4B and 4E with the control experiment.

The wave propagation speeds are better studied and compared in figure 5, in which time-longitude isopleths of meridional components of the wind are presented for the experiments with the three grids. At low latitudes, the troughs and ridges move eastward on all grids at about 23°/day or at nearly the theoretical rate. At high latitudes, however, the trough movement slows after 4 days, even in the control integration. There is actually some retrograde motion at 6 days in the low-resolution runs. With the modified Kurihara grid, the trough motion slows and reverses at an earlier day. Furthermore, this reversal occurs at a lower latitude. Figure 5 also illustrates the irregular character of the flow patterns computed on the modified Kurihara grid even more than the height field maps.

The mean zonal wind at 6 days is plotted against latitude in figure 6 for the three experiments. The initial wind profile is shown in this figure as a thin solid line. Notice that the initial zonal wind is 50 m/s from the west at the Equator and decreases monotonically to zero at the pole. The true divergent barotropic solution, best portrayed here by the dashed curve for the control run, exhibits a peak in the zonal westerlies of about 100 m/s at 13° latitude and a minimum of 20 m/s from the east at about 42° latitude. This profile is consistent with the presence of Lows that form at about 30° latitude. At low latitudes, the wind profile of the modified Kurihara-grid run is similar in shape to those for the latitude-longitude grids, but poleward of 25° the profile is irregular and differs greatly from the winds obtained from the latitude-longitude grids.

The zonal mean geopotential height after 6 days is plotted against latitude in figure 7 for the three barotropic
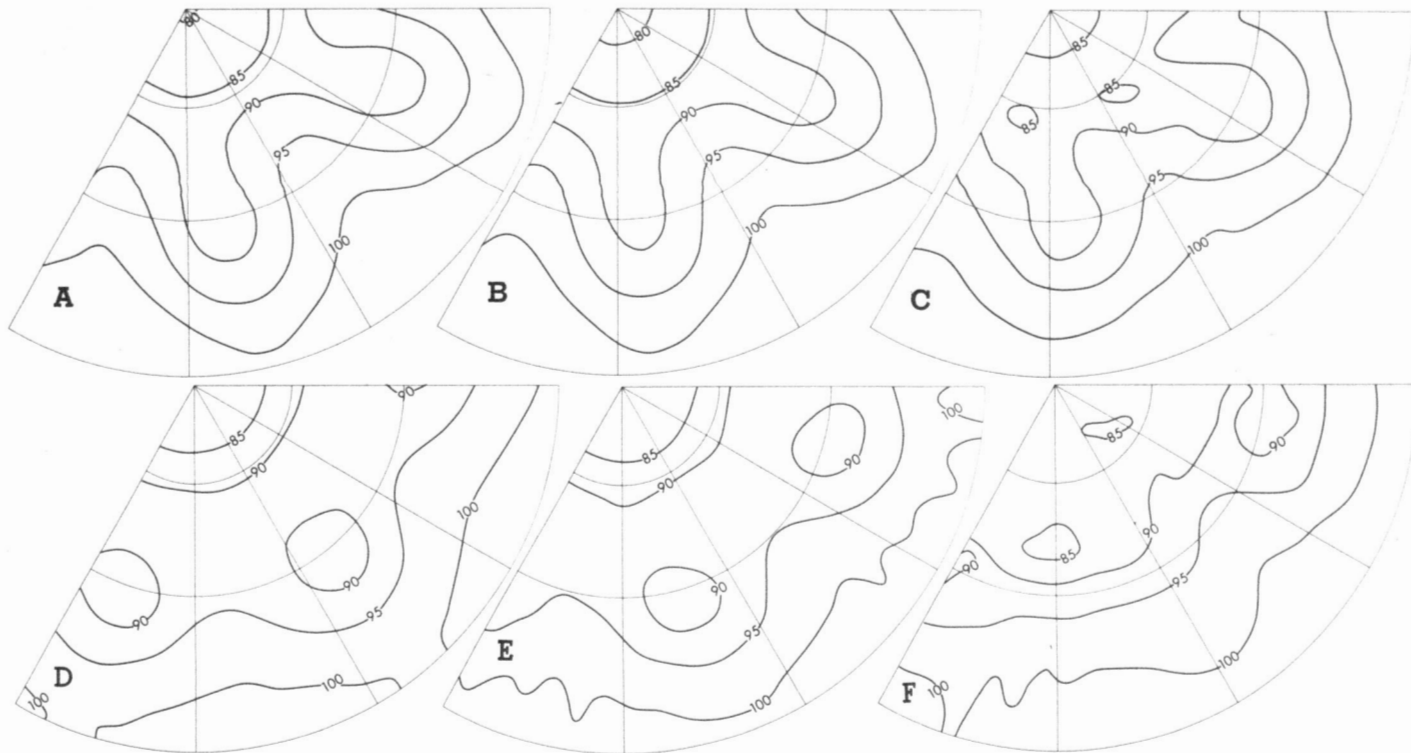
FIGURE 4.—Free-surface geopotential height fields (102.04 gpm) for day 3 (A–C) and day 6 (D–F) of sector time integrations on the control grid (A, D), the latitude-longitude grid (B, E), and on the modified Kurihara grid (C, F).
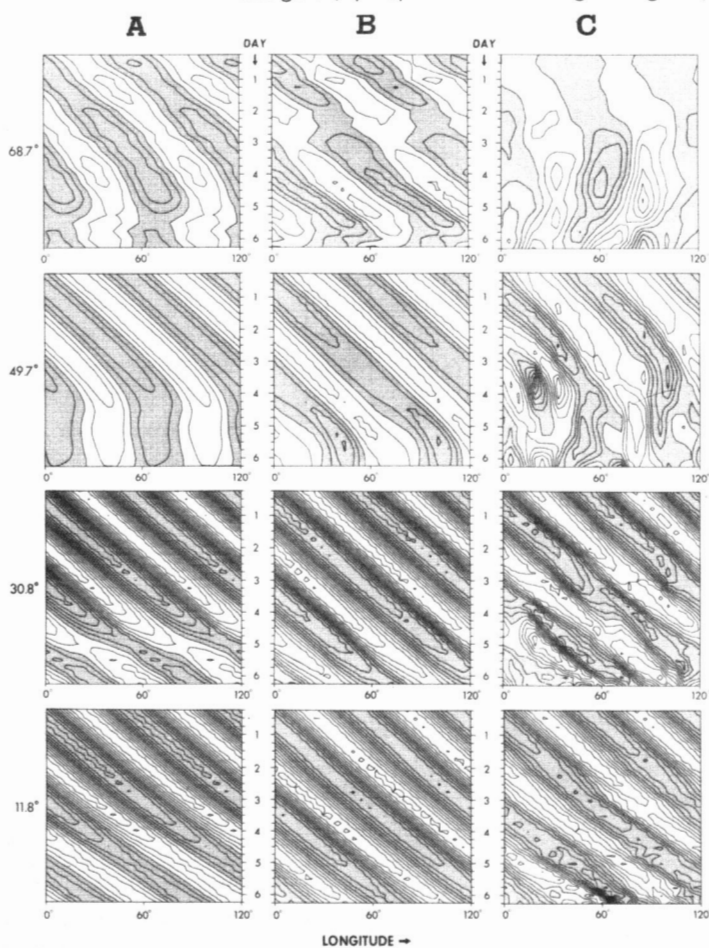

FIGURE 5.—Isopleths of meridional component of the wind in the longitude-time plane for the three-sector model experiments, (A) control run, (B) latitude-longitude grid run, and (C) modified Kurihara grid, for four selected latitudes, 11.8°, 30.8°, 49.7°, and 68.7°. Contour interval is 10 m/s and shaded areas are northward components.
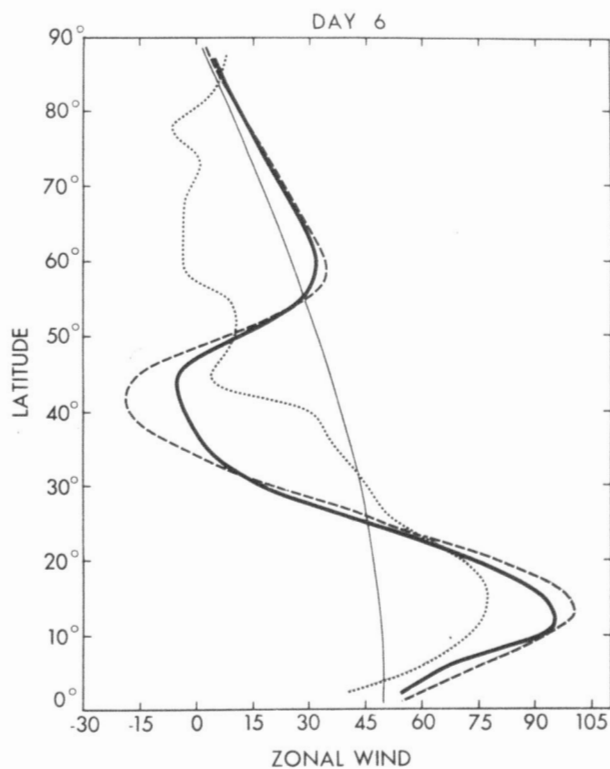

FIGURE 6.—Zonal wind speed (m/s) versus latitude for the initial data (light solid line) and for the three-sector model integrations; namely, control run (dashed line), latitude-longitude grid (heavy solid line), and modified Kurihara grid (dotted line), after 6 days.

experiments, along with the initial zonal distribution of geopotential. Notice the pronounced computational mode in the modified Kurihara-grid profile in polar regions. The polar heights computed on the modified Kurihara grid also tend to be much too high. As mentioned before,

higher than normal polar pressures have been characteristic of previous time integrations on the Kurihara grid. Figure 7 shows that the latitude-longitude grid appears to have corrected these problems. The close agreement of the zonal winds of the latitude-longitude grid experiment with those of the control run is consistent with the agreement in height profiles. The slightly flatter height profile obtained from the low-resolution, latitude-longitude grid accounts for the somewhat lower peaks in the westerlies of the Tropics and the lighter easterlies in middle latitudes as compared with the computations on the high-resolution control grid.

The mechanism for the development of rising heights near the poles in the modified Kurihara-grid time integration is clear from figures 5–7. The difference in phase speeds of the waves between latitudes, caused by the decreasing east–west resolution toward the poles, introduces errors in the momentum transport in the model. This, in turn, creates an unrealistic mean zonal wind distribution, which requires higher than normal heights in polar regions by the geostrophic wind relationship. Marked reduction in the difference in wave propagation speeds between latitudes, obtained on the latitude-longitude grid, corrects most of this tendency toward improper heights in polar regions.

5. TEST WITH CROSS-POLAR FLOW

The experiments described in the last section do not test the performance of the latitude-longitude grid in the case of strong winds across the pole because use of the 120° sector with cyclic continuity prohibits the introduction or development of cross-polar flow. Dey (1969) pointed out that divergence fields in the vicinity of the poles are inaccurately computed on the Kurihara grid when there is strong cross-polar flow. Since this situation is common in the atmosphere, we tested the barotropic model on a case in which wind was allowed to blow across the pole.

To perform this test, we expanded the sector model into a hemisphere. In the low-resolution, hemispheric, latitude-longitude grid, there are 19 rows of data as before; but the number of points in a latitude circle is 76, one more than three times the number in the 120° sector. The initial conditions for this experiment were again those of Phillips (1959) but with the wave number specified as 1 instead of 6. This defines a single vortex offset from the pole. The initial geopotential height for this case is shown in figure 8A. The wind speed across the pole is 50 m/s initially.

The barotropic model was time-integrated on the low-resolution grid described previously and on a high-resolution, hemispheric, latitude-longitude grid with twice the number of rows (38) and four times as many gridpoints (5,776) as in the former grid. The resolutions of these two grids are almost identical to those of the low- and high-resolution sector grids, respectively. The time-step lengths are the same as before (600 and 12 s, respectively). The high-resolution run was made as a control experiment to gage the accuracy of computations of the Fourier-filtered, low-resolution grid model. For this reason, no filtering is done on the time integration computed on the
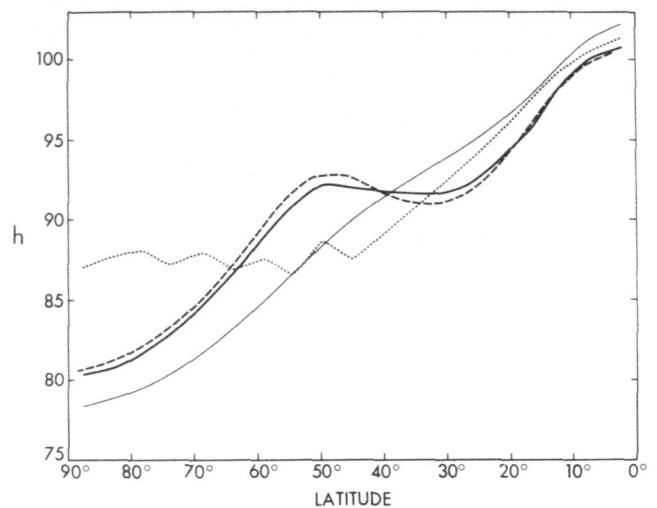

FIGURE 7.—Zonal mean geopotential height (102.04 gpm) versus latitude for the initial data (light solid line) and for the three-sector model time integrations; namely, control run (dashed line), latitude-longitude grid (heavy solid line), and modified Kurihara grid (dotted line), after 6 days.

finer grid, thus explaining the very short time steps used. The maximum wave number permitted at each latitude in the filtered low-resolution run is obtained from eq (2).

Both time integrations were extended to 6 days. The final distributions of geopotential height derived on the two grids are shown in figure 8. After 6 days, the low-resolution results and the control run still appear similar. In fact, the vortex has simply moved around the pole with little change in shape. The trough line has retrograded at the rate of about 53°/day. Since the intervening distributions are not shown, the westward motion is not apparent in figure 8 because the vortex has almost returned to its original position. The analytically derived rate of retrograde motion for nondivergent flow is 94.4°/day. Apparently, in the model computations, divergence has slowed the trough motion to about half of the theoretical rate. The trough in the control run moved about 1 percent faster than in the low-resolution run.

The strong flow across the pole does not seem to cause the Fourier-filtered, latitude-longitude grid model any difficulty, and the results appear to be accurate as evidenced by the high-resolution control time integration.

6. THE BAROCLINIC MODEL

A global, nine-level, atmospheric general circulation model with surface topography is used for this test. The primitive equations of motion in spherical coordinates are time-integrated on a global, latitude-longitude (GLL) grid. Except for the grid system, the structure of the baroclinic test model is identical to that of the general circulation model described in detail by Holloway and Manabe (1971) (hereafter referred to as study HM). The grid system used in that study was the low-resolution Kurihara grid having 24 rows of gridpoints between the poles and the Equator (designated as N24 in study HM).

Fourier space filtering of the predicted variables is done on the GLL grid. The procedure for filtering is identical
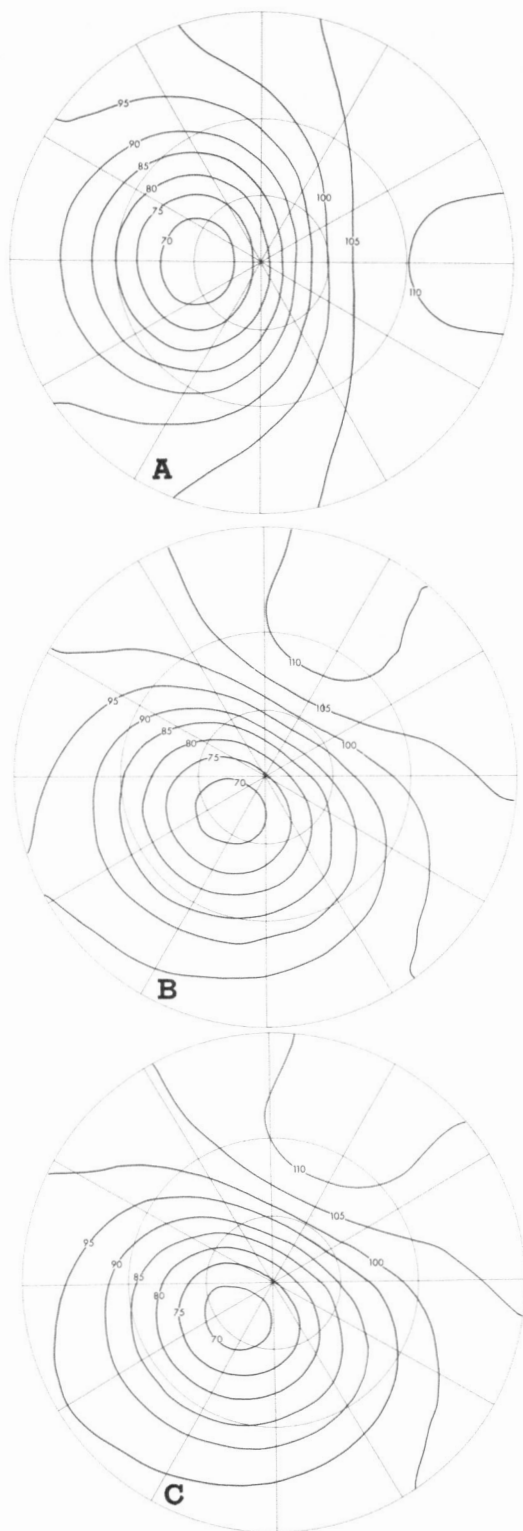
FIGURE 8.—Free-surface geopotential height distribution (102.04 gpm) for the hemispheric grid models for (A) initial field, (B) day 6 of the low-resolution latitude-longitude grid time integration, and (C) day 6 of the high-resolution control run.

TABLE 2.—*Maximum wave number and east–west grid spacing tabulated against latitude for the GLL grid baroclinic model test*

Latitude (deg.)	Maximum wave number	Grid spacing (km)
2. 4	33	606
7. 1	33	602
11. 8	33	594
16. 6	33	581
21. 3	33	565
26. 1	33	545
30. 8	33	521
35. 5	33	494
40. 3	33	463
45. 0	30	472
49. 7	26	498
54. 5	23	506
59. 2	19	539
63. 9	17	517
68. 7	14	520
73. 4	11	519
78. 2	8	513
82. 9	5	495
87. 6	2	414

of topography-induced gravity waves in the time integration.

The grid system for the GLL grid model is an expanded version of the latitude-longitude grid used for the barotropic model (fig. 1) with slightly less east–west resolution. Each latitude circle contains 66 gridpoints, and each hemisphere has 19 rows of gridpoints between the Equator and the pole. The north–south grid distance is 527 km everywhere. The east–west grid spacing at low latitudes $(\theta<45°)$ is given in table 2. At latitudes where the space filtering is done, the table gives an effective east–west grid distance that is half of the minimum wavelength permitted by the filtering procedure. Also listed in table 2 is the maximum wave number at each latitude.

The initial condition for the numerical time integration of the GLL grid model is data interpolated from day 302 of the N24 Kurihara grid model experiment. The integration was terminated after 64 days, and the final 20-day period was time averaged. During this period, the model atmosphere had not yet reached a state of thermal equilibrium. The results presented here, however, should be similar to the mean model atmosphere that would have been attained on the GLL grid.

In the grid system that was used for the N24 Kurihara grid model, the gridpoints at each latitude are staggered with respect to those at adjacent latitudes. There are 96 gridpoints along the Equator, decreasing to only four gridpoints in the latitude circles nearest the poles. The north–south grid distance is 417 km everywhere, and the east–west grid spacing increases from 417 km at the Equator to 650 km near the poles. Complete details of that computational grid are given in study HM. The east–west resolutions of the N24 Kurihara grid and the N19 GLL grid are comparable, but the north–south resolution of the N24 Kurihara grid is actually better than that of the GLL grid.

to that used for the barotropic model, as discussed in section 2, except that the space filtering is done only from 45° latitude to the poles for the global experiment. The length of the time step remained unchanged at 10 min with this modification. It is necessary to space-filter the surface topography in exactly the same way as the predicted variables in this model to prevent the occurrence

The discussion of results from the two different grids will be confined to the sea-level pressure distribution. Simulation of this feature was one of the severest shortcomings of the Kurihara grid model, as pointed out in study HM.

The zonally averaged sea-level pressure versus latitude for the GLL grid model and for the N24 Kurihara grid model is shown in figure 9. Also shown in this figure is the observed pressure distribution for January from Crutcher and Meserve (1970) for the Northern Hemisphere, and from Taljaard et al. (1969) for the Southern Hemisphere. Several interesting features are evident. In the Northern Hemisphere polar region, the GLL grid model has mean sea-level pressures that are nearly 30 mb lower than those of the Kurihara grid model. The Northern Hemisphere subtropical high-pressure belt has also intensified and moved closer to the observed profile. These encouraging results are not reflected in the Southern Hemisphere, however, where the results from the GLL grid are only a slight improvement over those from the Kurihara grid model. Evidently, the mechanism for producing the intense storm belt along the periphery of the Antarctic continent is not related to the choice of grid configuration. The reasons for this unrealistic feature are still being investigated, but they may be partly related to the coarseness of the grid resolution. In study HM, figure 7 shows that the meridional surface pressure gradient is increased in midlatitudes when the horizontal grid resolution is increased.

The GLL grid model has zonal mean sea-level pressures in the Northern Hemisphere subpolar region that are lower than the observed by as much as 7 mb. This feature is caused by a very intense Aleutian Low in the model. Because of the imposed insolation for January throughout the model integration, the Northern Hemisphere polar region becomes abnormally cold with excessive snow cover over the continents. As a result, the land–sea temperature contrast is enhanced, and this exaggerates the development of the Aleutian Low.

7. CONCLUDING REMARKS

There is considerable improvement in the results of the barotropic model, integrated on the sector latitude-longitude grid, over results from the same equations solved on the modified Kurihara grid with comparable resolution. The appearance of the height fields after 6 days, obtained from the latitude-longitude grid, is much closer to the control run results than those obtained on the modified Kurihara grid. The errors produced by the modified Kurihara grid are most pronounced near the poles, in agreement with other models using this type of grid.

The time integration of the barotropic model on the low-resolution, hemispheric, latitude-longitude grid is almost identical with the one performed on the high-resolution control grid without the use of Fourier filtering. Despite the strong flow across the poles in the initial data, no apparent errors or irregularities occurred during the 6-day run.
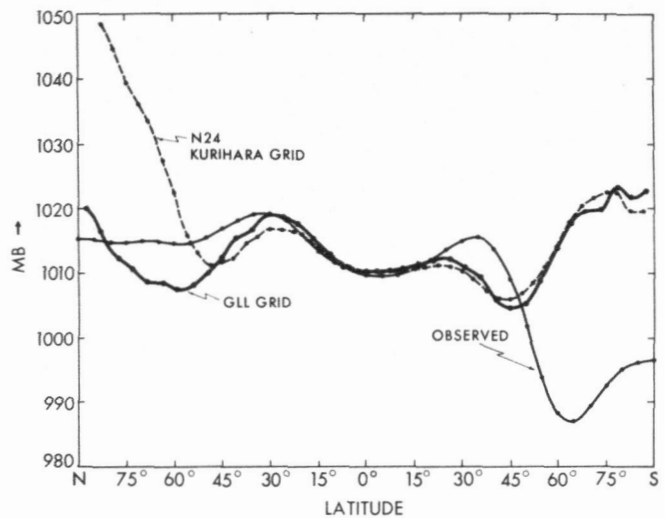
FIGURE 9.—Latitudinal distributions of the zonal mean sea-level pressures derived for the actual atmosphere (thin solid line) and computed by the global latitude-longitude grid model (heavy solid line) and by the N24 Kurihara grid model (dashed line).

The results obtained by integrating the baroclinic model on the global latitude-longitude grid are also better than those simulated on the Kurihara grid system in respect to the feature of the time integration most subject to error on the latter grid; namely, sea-level pressure in high latitudes.

APPENDIX 1: STABILITY ANALYSIS FOR LATITUDE-LONGITUDE GRID

To show how filtering permits the retention of a normal-length time step even in the region of small spacing near the poles of the latitude-longitude grid, one must only perform a stability analysis on a simple system of equations. Consider the following equations, which govern a one-dimensional shallow water wave:

$$\frac{\partial u}{\partial t}+g\,\frac{\partial h}{\partial x}=0 \qquad (10)$$

and

$$\frac{\partial h}{\partial t}+H\,\frac{\partial u}{\partial x}=0 \qquad (11)$$

where u is velocity, t is time, g is the acceleration of gravity, h is the height of the disturbed fluid, x is the space dimension, and H is the total depth of the fluid at rest.

If u and h are defined on the same grid, the finite-difference versions of eq (10) and (11) are as follows:

$$\frac{\partial u_{l+1}}{\partial t}+\frac{g}{2d}\,(h_{l+2}-h_l)=0 \qquad (12)$$

and

$$\frac{\partial h_l}{\partial t}+\frac{H}{2d}\,(u_{l+1}-u_{l-1})=0 \qquad (13)$$

where l is the gridpoint index and d is the grid spacing. Let

$$u_{l+1}\equiv\hat{u}e^{ik(l+1)d} \qquad (14)$$

and

$$h_l \equiv \hat{h} e^{ikld}. \tag{15}$$

Substituting the above definitions into eq (12) and (13), we obtain the following relation after differentiating the modified eq (12) with respect to time and combining these two equations into one:

$$\frac{\partial^2 \hat{u}}{\partial t^2} = -\Omega^2 \hat{u} \tag{16}$$

where

$$\Omega = cd^{-1} \sin (kd) \tag{17}$$

and

$$c^2 = gH. \tag{18}$$

The finite-difference version of eq (16) in centered leapfrog form is

$$(2\Delta t)^{-2}(u_{\tau+2} + u_{\tau-2} - 2u_\tau) = -\Omega^2 \hat{u}_\tau. \tag{19}$$

Let $u_\tau \equiv A e^{i\nu\tau\Delta t}$ where Δt is the time-step length. After substituting this definition into eq (19), we get

$$\lambda^2 + \lambda^{-2} - 2 = -(2\Delta t \Omega)^2 \tag{20}$$

where

$$\lambda \equiv \frac{\hat{u}_{\tau+1}}{\hat{u}_\tau} = e^{i\nu\Delta t}. \tag{21}$$

Solving eq (20) for λ, we obtain

$$\lambda = \pm i\Omega\Delta t \pm \sqrt{1 - \Omega^2 \Delta t^2}. \tag{22}$$

If $|\Omega\Delta t|$ is less than one, then the absolute value of the complex ratio λ is equal to one, which represents neutral stability. However, if $|\Omega\Delta t|$ is greater than one, the absolute value of λ is greater than one, and the equations are amplifying and unstable.

Using eq (17) and manipulating factors, we obtain the stability criterion

$$|c|\Delta t < \frac{L}{2\pi \left[\dfrac{\sin (kd)}{kd}\right]} \tag{23}$$

where L is the wavelength corresponding to wave number k according to the formula

$$L = 2\pi k^{-1}. \tag{24}$$

Therefore, if the minimum value of L is increased by filtering, the time-step length, Δt, may be increased without creating linear instability.

APPENDIX 2: FINITE-DIFFERENCE VERSION OF BAROTROPIC MODEL EQUATIONS

The finite-difference versions of the equations given in section 3 are as follows:

$$\left(\frac{\partial hu}{\partial t}\right)_{i,j} = -D(u)_{i,j} + C_{i,j} h_{i,j} v_{i,j} - \frac{g}{4} (h_{i+1,j}^2 - h_{i-1,j}^2) w_{C_j}, \tag{25}$$

$$\left(\frac{\partial hv}{\partial t}\right)_{i,j} = -D(v)_{i,j} - C_{i,j} h_{i,j} u_{i,j}$$
$$- \frac{g}{4} [(h_{i,j+1}^2 - h_{i,j}^2) w_{N_j} + (h_{i,j}^2 - h_{i,j-1}^2) w_{S_j}], \tag{26}$$

and

$$\left(\frac{\partial h}{\partial t}\right)_{i,j} = -D(1)_{i,j} \tag{27}$$

where the divergence operator is defined as

$$D(\phi)_{i,j} = \left(\overline{\overline{h}_{i+1/2,j}^x \overline{u}_{i+1/2,j}^x \overline{\phi}_{i+1/2,j}^x} - \overline{\overline{h}_{i-1/2,j}^x \overline{u}_{i-1/2,j}^x \overline{\phi}_{i-1/2,j}^x}\right) w_{C_j}$$
$$+ \overline{\overline{h}_{i,j+1/2}^y \overline{v}_{i,j+1/2}^y \overline{\phi}_{i,j+1/2}^y} w_{N_j} - \overline{\overline{h}_{i,j-1/2}^y \overline{v}_{i,j-1/2}^y \overline{\phi}_{i,j-1/2}^y} w_{S_j}. \tag{28}$$

In eq (28), the overbar operators are defined as

$$\overline{\alpha_{i,j}}^x = \frac{1}{2} (\alpha_{i+1/2,j} + \alpha_{i-1/2,j}) \tag{29}$$

and

$$\overline{\alpha_{i,j}}^y = \frac{1}{2} (\alpha_{i,j+1/2} + \alpha_{i,j-1/2}). \tag{30}$$

In eq (25) and (26), the Coriolis coefficient is given by

$$C_{i,j} = f_j + a^{-1} u_{i,j} \tan \theta_j. \tag{31}$$

The grid box weights (central, north, or south) are computed by the relations

$$w_{C_j} = \Delta\theta I_j \left[4\pi a \sin\left(\frac{\Delta\theta}{2}\right) \cos \theta_j\right]^{-1} \tag{32}$$

and

$$w_{(N/S)_j} = \cos \theta_{j\pm1/2} \left[2a \sin\left(\frac{\Delta\theta}{2}\right) \cos \theta_j\right]^{-1} \tag{33}$$

where $\Delta\theta = \frac{1}{2}\pi N^{-1}$, I_j is the number of gridpoints in row j, and N is the number of gridpoints between the pole and the Equator. The indices i and j increase eastward and northward, respectively. More details on the box method used in formulating these equations are given by Kurihara and Holloway (1967).

In the modified Kurihara grid, where each box generally has more than one north and one south contiguous neighbor, the above equations are modified to allow for contributions from more than one neighbor in each direction. These contributions are weighted by the relative lengths of the interfaces between the central box and the two or three neighbors in the direction considered.

APPENDIX 3: COMPUTATIONAL CONSIDERATIONS

In regard to accuracy of meteorological results, the latitude-longitude grid is a better grid system on which to solve the finite-difference equations for our models than a Kurihara-type grid of comparable resolution.

No penalty in decreased time step is required for computational stability in the latitude-longitude grid time integration if the Fourier space filtering is done properly.

The latitude-longitude grid model, however, runs more slowly on the computer than the modified Kurihara grid model for two reasons. First, there are more than one and a half times as many gridpoints in a latitude-longitude grid than in the modified Kurihara grid. This handicap is, nevertheless, nearly offset by the fact that a typical Kurihara grid box generally has six surrounding gridpoints, whereas all boxes on the latitude-longitude grid have only four contiguous boxes except at the poles, where there are only three.

Secondly, the latitude-longitude grid time integration runs slower than that on the Kurihara grid because of the additional computer time required by the Fourier filtering. Fast Fourier techniques are now available for performing Fourier analyses on computers rapidly and efficiently. To take advantage of these new methods, one must be sure that the number of points per row is a power of two or at least divisible by four. Unfortunately, only two of the grids used in this paper satisfied this requirement. Efficiently programmed, the filtering method described here should not need more than 10 percent more computer time than that required for the rest of the time integration in a typical general circulation model.

Furthermore, the next generation of computers will have much more parallelism than the computers on which these experiments were done. Models with rectangular arrays of data will run much more efficiently on the new machines than those with nonrectangular grids. It is possible that on these computers no significant machine time penalty will result from solving model equations at the additional polar gridpoints on the latitude-longitude grids described here.

Even if computation time on latitude-longitude grids cannot be reduced to that required on other global grids, the advantage of more accurate time integrations of model equations is ample justification for using the new grid system. Furthermore, programming a computer for a model solved on a latitude-longitude grid is easier than on most other global grid systems. Simplicity of programming is accompanied not only by reduced human effort in preparing the model for the computer, but also by greater computational efficiency on the machine.

REFERENCES

Crutcher, Harold L., and Meserve, J. M., "Selected Level Heights, Temperatures, and Dew Points for the Northern Hemisphere," *NAVAIR* 50–1C–52, U.S. Naval Weather Service, Washington, D.C., Jan. **1970**, 8 pp. and numerous charts.

Dey, Clifford H., "A Note on Global Forecasting With the Kurihara Grid," *Monthly Weather Review*, Vol. 97, No. 8, Aug. **1969**, pp. 597–601.

Gates, W. Lawrence, Batten, E. S., Kahle, A. B., and Nelson, A. B., "A Documentation of the Mintz-Arakawa Two-Level Atmospheric General Circulation Model," *Rand Corporation Report* No. R–877–ARPA, Santa Monica, Calif., Dec. **1971**, 408 pp.

Grimmer, M., and Shaw, D. B., "Energy-Preserving Integrations of the Primitive Equations on the Sphere," *Quarterly Journal of the Royal Meteorological Society*, Vol. 93, No. 397, London, England, July **1967**, pp. 337–349.

Holloway, J. Leith, Jr., "Smoothing and Filtering of Time Series and Space Fields," *Advances in Geophysics*, Vol. 4, Academic Press, New York, N.Y., **1958**, pp. 351–390.

Holloway, J. Leith, Jr., and Manabe, Syukuro, "Simulation of Climate by a Global General Circulation Model: I. Hydrologic Cycle and Heat Balance," *Monthly Weather Review*, Vol. 99, No. 5, May **1971**, pp. 335–370.

Kurihara, Yoshio, "Numerical Integration of the Primitive Equations on a Spherical Grid," *Monthly Weather Review*, Vol. 93, No. 7, July **1965**, pp. 399–415.

Kurihara, Yoshio, and Holloway, J. Leith, Jr., "Numerical Integration of a Nine-Level Global Primitive Equations Model Formulated by the Box Method," *Monthly Weather Review*, Vol. 95, No. 8, Aug. **1967**, pp. 509–530.

Manabe, Syukuro, Smargorinsky, Joseph, Holloway, J. Leith, Jr., and Stone, Hugh M., "Simulated Climatology of a General Circulation Model With a Hydrologic Cycle: III. Effects of Increased Horizontal Computational Resolution," *Monthly Weather Review*, Vol. 98, No. 3, Mar. **1970**, pp. 175–212.

Matsuno, Taroh, "Numerical Integrations of Primitive Equations by Use of a Simulated Backward Difference Method," *Journal of the Meteorological Society of Japan*, Vol. 44, No. 1, Tokyo, Feb. **1966**, pp. 76–84.

Phillips, Norman A., "Numerical Integration of the Primitive Equations on the Hemisphere," *Monthly Weather Review*, Vol. 87, No. 9, Sept. **1959**, pp. 333–345.

Shuman, Frederick G., "On Certain Truncation Errors Associated With Spherical Coordinates," *Journal of Applied Meteorology*, Vol. 9, No. 4, Aug. **1970**, pp. 564–570.

Taljaard, J. J., van Loon, H., Crutcher, H. L., and Jenne, R. L., "Climate of the Upper Air: Part 1. Southern Hemisphere, Volume 1. Temperatures, Dew Points, and Heights at Selected Pressure Levels," *NAVAIR* 50–1C–55, U.S. Naval Weather Service, Washington, D.C., Sept. **1969**, 6 pp. plus 134 figures.

Umscheid, Ludwig, Jr., and Sankar-Rao, M., "Further Tests of a Grid System for Global Numerical Prediction," *Monthly Weather Review*, Vol. 99, No. 9, Sept. **1971**, pp. 686–690.

Vanderman, Lloyd W., "Global Forecasts on a Latitude-Longitude Grid With Primitive Equation Models," *Proceedings of the International Seminar of Tropical Meteorology, Campinas, S.P., Brazil, September 25-October 10, 1969*, Escritorio de Meteorologia (M.A.), Brasilia, Brazil, **1970**, pp. 233–269.

Vanderman, Lloyd W., "Forecasting With a Global, Three-Layer, Primitive-Equation Model," *Monthly Weather Review*, Vol. 100, No. 12, Dec. **1972**, pp. 856–868.